4-23-2018

Cdc42-dependent modulation of rigidity sensing and cell spreading in tumor repopulating cells

Farhan Chowdhury
farhan.chowdhury@siu.edu

Sultan Doganay

Benjamin J. Leslie

Rishi Singh

Kshitij Amar

See next page for additional authors

Recommended Citation
Chowdhury, Farhan, Doganay, Sultan, Leslie, Benjamin J., Singh, Rishi, Amar, Kshitij, Talluri, Bhavana, Park, Seongjin, Wang, Ning and Ha, Taekjip. "Cdc42-dependent modulation of rigidity sensing and cell spreading in tumor repopulating cells." *Biochemical and Biophysical Research Communications* (Apr 2018). doi:10.1016/j.bbrc.2018.04.085.

Authors
Farhan Chowdhury, Sultan Doganay, Benjamin J. Leslie, Rishi Singh, Kshitij Amar, Bhavana Talluri, Seongjin Park, Ning Wang, and Taekjip Ha

Cdc42-dependent modulation of rigidity sensing and cell spreading in tumor repopulating cells

Farhan Chowdhury[1*], Sultan Doğanay[2†], Benjamin J. Leslie[3†‡], Rishi Singh[4], Kshitij Amar[1], Bhavana Talluri[1], Seongjin Park[2], Ning Wang[4], and Taekjip Ha[3,5]

[1]Department of Mechanical Engineering and Energy Processes, Southern Illinois University Carbondale, Carbondale, IL 62901, U.S.A.; [2]Department of Physics, University of Illinois at Urbana-Champaign, Urbana, IL 61801, U.S.A.; [3]Howard Hughes Medical Institute, Johns Hopkins University, Baltimore, MD, 21205, U.S.A.; [4]Department of Mechanical Science and Engineering, University of Illinois at Urbana-Champaign, Urbana, IL 61801, U.S.A.; [5]Department of Biophysics and Biophysical Chemistry, Johns Hopkins University, Baltimore, MD 21205, U.S.A. [†]Contributed equally. [‡]Present address: Department of Biology, The College of Wooster, Wooster, OH, U.S.A

*Correspondence: farhan.chowdhury@siu.edu (F.C.)

Abstract

Recently, a robust mechanical method has been established to isolate a small subpopulation of highly tumorigenic tumor repopulating cells (TRCs) from parental melanoma cells. In order to characterize the molecular and mechanical properties of TRCs, we utilized the tension gauge tether (TGT) single-molecule platform and investigated force requirements during early cell spreading events. TRCs required the peak single molecular tension of around 40 pN through integrins for initial adhesion like the parental control cells, but unlike the control cells, they did not spread and formed very few mature focal adhesions (FAs). Single molecule resolution RNA quantification of three Rho GTPases showed that downregulation of *Cdc42*, but not *Rac1*, is responsible for the unusual biophysical features of TRCs and that a threshold level of *Cdc42* transcripts per unit cell area is required to initiate cell spreading. Cdc42 overexpression rescued TRC spreading through FA formation and restored the sensitivity to tension cues such that TRCs, like parental control cells, increase cell spreading with increasing single-molecular tension cues. Our single molecule studies identified an unusual biophysical feature of suppressed spreading of TRCs that may enable us to distinguish TRC population from a pool of heterogeneous tumor cell population.

Keywords: Cell adhesion and spreading, tension gauge tethers, tumor repopulating cells, focal adhesions, smFISH.

1. INTRODUCTION

Cancer cells within a tumor ecosystem possess a remarkable capacity for self-renewal. Cancer stem cells, a small subpopulation of stem-cell-like-cells driving growth and progression of tumors, were first described in leukemia [1]. Following this work, several reports indicate the existence of cancer stem cells in solid tumors such as the breast [2], brain [3], skin [4], prostate [5], and the lungs [6]. However, evidence for the existence of cancer stem cells in solid tumors has been rather controversial primarily due to unreliably expressed antigen based selection techniques [7,8]. This prompted the need for the development of a robust technique to isolate a highly tumorigenic subpopulation of cancer cells. Recently, we successfully isolated a small fraction of highly tumorigenic cells, which we termed tumor repopulating cells (TRCs), from the B16-F1 melanoma cell line by culturing them in soft-3D-fibrin gels [9]. However, very little is known about the biophysical characteristics of such tumorigenic cells. In this study, we utilize a number of single-molecule techniques including single molecule fluorescence in situ hybridization (smFISH) [10] and our recently developed tension gauge tether (TGT) technique [11] to reveal the molecular and mechanical features of TRCs.

2. MATERIALS and METHODS

2.1 Cell culture

Melanoma cell lines B16-F1 and B16-F10 cells were maintained in rigid culture dishes with high-glucose DMEM (Invitrogen) cell culture medium containing 10% FBS (Hyclone) at 37 °C with 5% CO_2. The medium was supplemented with 2 mM L-glutamine, 1 mM sodium pyruvate, and 50 μg/ml penicillin-streptomycin. Soft 3D fibrin gels (90 Pa) were prepared as

described previously [9]. TRCs from these cell lines were grown in soft 3D fibrin gels using the same growth medium.

2.2 Surface functionalization

Tension gauge tethers of different tension tolerance were immobilized on passivated glass bottom dishes at a cyclic-RGDfK ligand density of ~ 600 ligands/μm^2 (one ligand in every 40 nm) as described elsewhere [11,12]. An earlier study showed that cell spreading and FA formations are not supported when the spacing between integrin binding sites is more than 58 nm [13]. Briefly, glass surfaces were incubated with biotinylated BSA (Sigma) for 20 min at room temperature, then washed with PBS and further incubated with NeutrAvidin (Thermo Fisher) for 10 min at room temperature. These surfaces were washed again with PBS and incubated with TGTs of different tension tolerance or biotinylated RGDfK peptides (Peptides International). Following surface functionalization, cells were seeded on the surface.

2.3 Cell area, volume, fluorescence intensity measurements

ImageJ (NIH) was used to measure projected cell spreading area, perimeter, and volume. 3D volume was estimated from the Z-stack images. Cell shape index (CSI), a geometric measure of circularity, is a non-dimensional parameter calculated based on the projected cell area and perimeter using the following relation, $\mathrm{CSI} = \frac{4*\pi*\mathrm{Area}}{\mathrm{Perimeter}^2}$. CSI values range from 0 to 1, 1 being a perfect circle while values less than 1 indicate complex spread pattern.

Statistical testing. All statistical analysis was carried out using a two-tailed Student's t-test unless noted otherwise.

3. RESULTS

3.1 TRCs do not spread on any TGT engineered surfaces

TGTs are rupturable DNA tethers with tunable tension tolerances, T_{tol} [11]. Here, one strand of the DNA is immobilized to a glass surface via biotin-neutravidin interactions and other strand is conjugated to cyclic-RGDfK peptide, specific to $\alpha_v\beta_3$ integrins [14]. T_{tol} is highest (56 pN) when the biotin is positioned on the opposite end of the rupturable duplex DNA tether (force is applied in a *shearing mode*) (Fig. 1a). T_{tol} progressively decreases to lowest value (12 pN) as the biotin is moved toward the same end of the duplex DNA tether (force is applied in an *unzipping mode*) (Fig. 1a). T_{tol} values can thus be tuned monotonically as a function of the distance between the biotin and the integrin ligand (Fig. 1a) [11,12,15]. Glass surfaces were passivated with biotinylated bovine serum albumin (BSA) prior to coating with neutravidin [12,16,17]. TGTs of varying T_{tol} or cyclic-RGDfK peptide (ruptures at significantly higher tension forces, >100 pN [12,18]) were then immobilized to the passivated surface through neutravidin-biotin linker (Fig. 1a).

Freshly isolated TRCs from soft 3D fibrin gel were plated on surface presenting TGTs of nominal T_{tol} values of 12, 23, 33, 43, 50, 56 or >100 pN (23 and 33 pN not shown). TRCs did not attach to surfaces with T_{tol} < 40 pN suggesting that they require about 40 pN peak force through integrins during initial cell adhesion. Interestingly, TRCs exhibited round morphology and projected cell area did not increase with increasing T_{tol} on any surface supporting cell adhesion, indicating their inability to spread in response to increasing mechanical stimuli across single molecular bonds (43, 50, 56, >100 pN) (Fig. 1 b, c).

Parental B16-F1 control cells also required 40 pN for initial cell adhesion, but unlike TRCs, they spread well on TGT surfaces, and cell spreading increased with increasing T_{tol}, suggesting that single molecular forces are sensed to promote cell spreading. (Supplementary Fig. 1; [12]). These data show that there is a fundamental difference in cell spreading between parental B16-F1 control cells and 3D fibrin selected TRCs.

To further quantify the differences in cell morphology, we computed cell shape index (CSI), a dimensionless parameter for geometric circularity measurement. TRCs exhibit CSI values close to 1 across all TGT surfaces (Fig. 1d). In contrast, parental B16-F1 control cells exhibited progressively lower CSI values as T_{tol} increased, due to complex cell spreading patterns [12]. Suppression of cell spreading in TRCs is not specific to B16-F1 cells because a similar difference was also observed between more aggressive B16-F10 melanoma cell line and their TRCs (Supplementary Fig. 2). TRCs also failed to spread on surfaces coated with natural ligands fibronectin or type-I collagen, showing that suppression of cell spreading is not due to the use of synthetic ligands (Supplementary Fig. 3).

3.2 Single-mRNA quantification shows altered expression of *RhoA* and *Cdc42* in TRCs

Because Rho-family small GTPases Rac1 and Cdc42 are known to regulate cell spreading, integrin clustering, and focal adhesion (FA) formation [19], we examined mRNA levels of Rac1 and Cdc42 in TRCs using qPCR. Transcription levels of both Rac1 and Cdc42 were significantly lower in TRCs compared to control cells (Supplementary Fig. 4). To understand and correlate phenotypic changes like cell spreading and FA formation with changes in gene expression at the single cell level, we utilized smFISH to visualize and quantify individual transcripts in fixed cells [10]. We imaged Rho-family small GTPases RhoA, Rac1, and Cdc42 mRNA molecules

simultaneously and quantified the mRNA transcripts from single cells (Fig. 2a). We observed positive correlations between *RhoA* and *Cdc42* (Fig. 2b, top panel) and between *RhoA* and *Rac1* (Fig. 2b, bottom panel) transcripts, with differences in absolute numbers of transcripts likely attributable to differences in cell volume. Since *RhoA* has an antagonistic relationship with *Rac1* and *Cdc42* [20], we quantified *RhoA* to *Cdc42* and *RhoA* to *Rac1* ratios in each cell (Fig. 2c). Average *RhoA* to *Rac1* ratios in the B16-F1 control cells and TRCs were similar, 2 and 3, respectively (Fig. 2b, bottom panel). However, the average ratio of *RhoA* to *Cdc42* in TRCs was ~2.7 fold higher than in control cells, potentially contributing to cell spreading suppression in TRCs. We also observed a large cell-cell variation of *RhoA* to *Cdc42* ratio in TRCs but not in control cells (Fig. 2c).

3.3 Many focal adhesions are formed by control melanoma cells but not TRCs

Since *Cdc42* is involved in integrin clustering and FA formation [19], we hypothesized that downregulation of *Cdc42* expression in TRCs may translate into fewer mature FAs. To test this, we utilized TIRF microscopy to monitor FAs in live cells expressing mCherry-vinculin. Control cells and TRCs were plated for 1 and 4 h on >100 pN passivated surfaces. In contrast to control cells, the number of mature FAs per individual TRC remained very low even after 4 h of cell plating, and failed to exhibit increases in area and polarization characteristic of mature FAs (Fig. 3a). To quantify mature FA characteristics, we compared differences in FA area and aspect ratio between control cells and TRCs (Figs. 3b,c and Supplementary Fig. 5). For control cells, the number of FAs per cell with an area $\geq 1.5\ \mu m^2$ increased by ~two fold between 1 hour and 4 hour of cell plating (Fig. 3b inset). In contrast, the number of FAs per cell with an area $\geq 1.5\ \mu m^2$ remained low and unchanged for TRCs (Fig. 3b inset). The average FA aspect ratio for control

cells increased by 40% between 1and 4 h of cell plating (Supplementary Fig. 5, left inset) but remained almost constant for TRCs (Supplementary Fig. 5, right inset).

3.4 Cdc42 restores cell spreading in TRCs

We next explored if cell spreading can be restored by transient overexpression of *Rac1* or *Cdc4*2 in TRCs. Transient overexpression of Cdc42-GFP restored cell spreading capacity in TRCs (Fig. 3d, left panel). More than 80% of cells, exhibiting GFP fluorescence, readily spread with typical filopodia-like extensions (Supplementary Fig. 6) and cells with low Cdc42-GFP fluorescence did not spread (Supplementary Fig. 7). In contrast, overexpression of Rac1-GFP did not restore normal cell spreading (Fig. 3d, right panel; Supplementary Figs. 6) and ~20% of cells spread partially with small lamellipodia-like protrusions (Supplementary Fig. 8). No cell spreading was observed in TRCs upon overexpression of RhoA-GFP or GFP-only (Supplementary Fig. 9).

We performed smFISH after transient transfection of *Cdc42* in TRCs to test if there exists a threshold of *Cdc42* to initiate TRC spreading (Fig. 3e, left). Spherical TRCs uniformly showed fewer than 25 transcripts per 100 μm^2 of projected cell area. This density indeed appears to be a threshold for cell spreading, as all transfected cells exceeded this density, and CSI decreased with increasing *Cdc42* density beyond this density (Fig. 3e, right). Conversely, knocking down *Cdc42* in parental B16-F1 control cells with 2 different siRNA constructs reversed their spread morphology, resulting in more than 80% Cdc42-knock down cells exhibiting round morphology similar to TRCs (Supplementary Fig. 10).

To determine the effect of Cdc42 on FA formation, we transiently transfected TRCs with a Cdc42-GFP plasmid and plated them on a >100 pN surface. After 4 h of cell plating, we fixed

and immunostained TRCs with primary anti-vinculin antibody to visualize FAs. Remarkably, TRCs transfected with Cdc42-GFP plasmid, in addition to spreading, were able to form focal adhesions (Supplementary Fig. 11). FA area quantification shows the number of adhesions similar to control cells (Supplementary Fig. 11b, Fig. 3b). Conversely, when *Cdc42* was knocked down in control cells with siRNA #1, they exhibited FA formation trend similar to TRCs (Supplementary Fig. 11b and Fig. 3c). Therefore, Cdc42 also has a role in FA assembly in TRCs in addition to TRC spreading.

3.5 Overexpression of Cdc42 rescues sensitivity to molecular tension cues

Finally, we tested whether the overexpression of Cdc42 can restore TRCs' sensitivity to mechanical cues. After transiently transfecting freshly isolated TRCs with Cdc42-GFP plasmid, GFP positive cells were collected using fluorescence activated cell sorting and applied to molecular tension surfaces with T_{tol} values of 43 pN, 56 pN, and >100 pN (Fig. 4a). Cdc42-overexpressing TRCs increased cell spreading with increasing T_{tol}, similar to control cells (Fig. 4b, blue bars). In addition, we computed CSI of TRCs on different T_{tol} surfaces and found that CSI values decreased with increasing T_{tol} suggesting the increase in protrusions leading to a more irregular cell spreading pattern with higher tension surfaces, similar to control cells (Fig. 4b, green bars).

4. DISCUSSION

Our TGT platform allows us to control the cell's mechanical environment at the single bond force level. This not only increased our understanding of integrin signaling [11,15,21] but also revealed force relevance of various mechanosensitive ligand-receptor interactions including

notch [17,22], selectins [23,24], T-cell receptors [25], and B cell receptor activation [26]. Because TRCs have been shown to depend on $\alpha_v\beta_3$ integrins to adhere and grow in a soft-3D-fibrin-gel system [9], we engineered TGT constructs to offer the same ligands (cyclic-RGDfK peptide) specific to $\alpha_v\beta_3$ integrins [14] to measure molecular forces exerted during cell adhesion and capture their cell spreading response. It remains to be explored if there is any difference in TRC adhesion and spreading through non-RGD integrins (e.g., LVD-binding integrins, αA domain integrins, and non- αA domain integrins) [27].

Previous studies have shown that cell spreading and gene regulation are modulated by the bulk stiffness of the underlying substrate [28,29]. However, the mechanism connecting the substrate stiffness to cell spreading and consequently fate-determination remain unresolved. Because cell spreading is known to be strongly coupled with cellular traction force generation [21,30], we recently investigated if capping the molecular forces at a predetermined value at the single integrin level has any impact on cell spreading and found B16-F1 control cells, together with many other cell lines, progressively increase spreading with the increase of single-molecular tension cues [12]. This evidence strongly suggests that ultimately the tension tolerance of single bonds can dictate the differential spreading response. Therefore, at the most fundamental level, the rigidity sensing and resultant changes in cell spreading can occur by sensing the single-molecular forces across ligand-receptor bonds. In this work, we showed that highly tumorigenic TRCs, a subpopulation of B16-F1 control cells, exhibit an unusual behavior of suppressed spreading. When we plated TRCs on different molecular tension tolerance surfaces, they did not change their spreading characteristics. The inability to spread and sense the tension cues are due to the reduced expression of *Cdc42*. Once *Cdc42* expression was restored, TRCs were able to spread through FA formation and exhibited molecular tension-dependent

spreading just like B16-F1 control cells. It remains to be tested if Cdc42 upregulation has any negative effect on the tumorigenicity of TRCs in animal models.

As TRCs do not spread, one can imagine that TRCs may exert a high cortical tension to limit the extent of cell spreading. However, cell stiffening response measurement as a function of the bulk stiffness of polyacrylamide hydrogels [31] showed that B16-F1 TRCs are much softer than the parent cell line suggesting cortical tension is much lower [31]. We also showed that TRCs stiffen with increasing substrate rigidity and such stiffening response is mediated by *Cdc42* [31]. In integrin-mediated mechanotransduction, downstream focal adhesion kinase (FAK) is one of the molecules that controls *Cdc42* activity [32]. Recently, downregulation of FAK has been reported to regulate histone 3 lysine residue 9 (H3K9) demethylation via *Cdc42* [33], providing a potential link between *Cdc42* and TRC self-renewal. However, the role of *Cdc42* in translating outside physical cues into meaningful intracellular signals and its contribution to regulating cell spreading and self-renewal was not well understood. In this work, we showed that *Cdc42* can control focal adhesion maturation and cell spreading in response to molecular tension cues received through single integrins, and that both processes are severely perturbed in TRCs. Future studies will reveal whether this unique feature is shared by all TRCs irrespective of tumor origin.

ACKNOWLEDGEMENTS

We thank Paul Selvin for access to a TIRF microscope. We also thank Arash Tajik, Youhua Tan, Isaac T. S. Li, Jihye Seong, Sang-Hak Lee, and Xuefeng Wang for technical help and discussion. Yingxiao Wang generously provided a mCherry-vinculin plasmid. Cdc42 (ID # 12975), Rac1 (ID # 12980), and RhoA (ID #23224) plasmids were obtained from Addgene. F.C.

acknowledges SIUC and Institute for Genomic Biology (University of Illinois at Urbana-Champaign). This work was partly supported by NIH GM072744 (N.W.). T.H. is an investigator with the Howard Hughes Medical Institute.

AUTHOR CONTRIBUTIONS

F.C., N.W., T.H. conceived the project and designed the experiments. F.C., S.D., B.L., R.S., K.A., B.T., S.P. performed experiments and/or analyzed data. R.S. developed image analysis suite for focal adhesion tracking. F.C., N.W., and T.H. wrote the manuscript with feedback from all authors.

SUPPLEMENTARY MATERIALS

Supplementary information includes experimental procedures, tables, figures, and references.

REFERENCES

[1] D. Bonnet, J.E. Dick, Human acute myeloid leukemia is organized as a hierarchy that originates from a primitive hematopoietic cell, Nat Med 3 (1997) 730-737.

[2] M. Al-Hajj, M.S. Wicha, A. Benito-Hernandez, S.J. Morrison, M.F. Clarke, Prospective identification of tumorigenic breast cancer cells, Proc Natl Acad Sci U S A 100 (2003) 3983-3988.

[3] S.K. Singh, I.D. Clarke, M. Terasaki, V.E. Bonn, C. Hawkins, J. Squire, P.B. Dirks, Identification of a cancer stem cell in human brain tumors, Cancer Res 63 (2003) 5821-5828.

[4] D. Fang, T.K. Nguyen, K. Leishear, R. Finko, A.N. Kulp, S. Hotz, P.A. Van Belle, X. Xu, D.E. Elder, M. Herlyn, A tumorigenic subpopulation with stem cell properties in melanomas, Cancer Res 65 (2005) 9328-9337.

[5] A.T. Collins, P.A. Berry, C. Hyde, M.J. Stower, N.J. Maitland, Prospective identification of tumorigenic prostate cancer stem cells, Cancer Res 65 (2005) 10946-10951.

[6] A. Eramo, F. Lotti, G. Sette, E. Pilozzi, M. Biffoni, A. Di Virgilio, C. Conticello, L. Ruco, C. Peschle, R. De Maria, Identification and expansion of the tumorigenic lung cancer stem cell population, Cell Death Differ 15 (2008) 504-514.

[7] E. Quintana, M. Shackleton, M.S. Sabel, D.R. Fullen, T.M. Johnson, S.J. Morrison, Efficient tumour formation by single human melanoma cells, Nature 456 (2008) 593-598.

[8] E. Quintana, M. Shackleton, H.R. Foster, D.R. Fullen, M.S. Sabel, T.M. Johnson, S.J. Morrison, Phenotypic heterogeneity among tumorigenic melanoma cells from patients that is reversible and not hierarchically organized, Cancer Cell 18 (2010) 510-523.

[9] J. Liu, Y. Tan, H. Zhang, Y. Zhang, P. Xu, J. Chen, Y.-C. Poh, K. Tang, N. Wang, B. Huang, Soft fibrin gels promote selection and growth of tumorigenic cells, Nature Materials 11 (2012) 734-741.

[10] A. Raj, P. van den Bogaard, S.A. Rifkin, A. van Oudenaarden, S. Tyagi, Imaging individual mRNA molecules using multiple singly labeled probes, Nat Methods 5 (2008) 877-879.

[11] X. Wang, T. Ha, Defining Single Molecular Forces Required to Activate Integrin and Notch Signaling, Science 340 (2013) 991-994.

[12] F. Chowdhury, I.T.S. Li, B.J. Leslie, S. Doğanay, R. Singh, X. Wang, J. Seong, S.-H. Lee, S. Park, N. Wang, T. Ha, Single molecular force across single integrins dictates cell spreading, Integrative Biology 7 (2015) 1265-1271.

[13] M. Arnold, E.A. Cavalcanti-Adam, R. Glass, J. Blümmel, W. Eck, M. Kantlehner, H. Kessler, J.P. Spatz, Activation of Integrin Function by Nanopatterned Adhesive Interfaces, Chemphyschem 5 (2004) 383-388.

[14] M. Aumailley, M. Gurrath, G. Muller, J. Calvete, R. Timpl, H. Kessler, Arg-Gly-Asp constrained within cyclic pentapeptides. Strong and selective inhibitors of cell adhesion to vitronectin and laminin fragment P1, FEBS Lett 291 (1991) 50-54.

[15] M. Roein-Peikar, Q. Xu, X. Wang, T. Ha, Ultrasensitivity of Cell Adhesion to the Presence of Mechanically Strong Ligands, Physical Review X 6 (2016).

[16] R. Roy, S. Hohng, T. Ha, A practical guide to single-molecule FRET, Nat Methods 5 (2008) 507-516.

[17] F. Chowdhury, I.T.S. Li, T.T.M. Ngo, B.J. Leslie, B.C. Kim, J.E. Sokoloski, E. Weiland, X. Wang, Y.R. Chemla, T.M. Lohman, T. Ha, Defining Single Molecular Forces Required for Notch Activation Using Nano Yoyo, Nano Letters 16 (2016) 3892-3897.

[18] V.T. Moy, E.L. Florin, H.E. Gaub, Intermolecular forces and energies between ligands and receptors, Science 266 (1994) 257-259.

[19] C. Ballestrem, B. Hinz, B.A. Imhof, B. Wehrle-Haller, Marching at the front and dragging behind: differential alphaVbeta3-integrin turnover regulates focal adhesion behavior, J Cell Biol 155 (2001) 1319-1332.

[20] M. Machacek, L. Hodgson, C. Welch, H. Elliott, O. Pertz, P. Nalbant, A. Abell, G.L. Johnson, K.M. Hahn, G. Danuser, Coordination of Rho GTPase activities during cell protrusion, Nature 461 (2009) 99-103.

[21] N. Wang, E. Ostuni, G.M. Whitesides, D.E. Ingber, Micropatterning tractional forces in living cells, Cell Motil Cytoskeleton 52 (2002) 97-106.

[22] V.C. Luca, B.C. Kim, C. Ge, S. Kakuda, D. Wu, M. Roein-Peikar, R.S. Haltiwanger, C. Zhu, T. Ha, K.C. Garcia, Notch-Jagged complex structure implicates a catch bond in tuning ligand sensitivity, Science 355 (2017) 1320-1324.

[23] I.T.S. Li, T. Ha, Y.R. Chemla, Mapping cell surface adhesion by rotation tracking and adhesion footprinting, Scientific Reports 7 (2017) 44502.

[24] X. Wang, Z. Rahil, I.T.S. Li, F. Chowdhury, D.E. Leckband, Y.R. Chemla, T. Ha, Constructing modular and universal single molecule tension sensor using protein G to study mechano-sensitive receptors, Scientific Reports 6 (2016).

[25] Y. Liu, L. Blanchfield, V.P.-Y. Ma, R. Andargachew, K. Galior, Z. Liu, B. Evavold, K. Salaita, DNA-based nanoparticle tension sensors reveal that T-cell receptors transmit defined pN forces to their antigens for enhanced fidelity, Proceedings of the National Academy of Sciences 113 (2016) 5610-5615.

[26] Z. Wan, X. Chen, H. Chen, Q. Ji, Y. Chen, J. Wang, Y. Cao, F. Wang, J. Lou, Z. Tang, W. Liu, The activation of IgM- or isotype-switched IgG- and IgE-BCR exhibits distinct mechanical force sensitivity and threshold, Elife 4 (2015).

[27] J.D. Humphries, A. Byron, M.J. Humphries, Integrin ligands at a glance, J Cell Sci 119 (2006) 3901-3903.

[28] A.J. Engler, S. Sen, H.L. Sweeney, D.E. Discher, Matrix elasticity directs stem cell lineage specification, Cell 126 (2006) 677-689.

[29] J. Solon, I. Levental, K. Sengupta, P.C. Georges, P.A. Janmey, Fibroblast adaptation and stiffness matching to soft elastic substrates, Biophys J 93 (2007) 4453-4461.

[30] C.A. Reinhart-King, M. Dembo, D.A. Hammer, The dynamics and mechanics of endothelial cell spreading, Biophys J 89 (2005) 676-689.

[31] Y. Tan, Tajik, A., Chen, J., Jia, Q., Chowdhury, F., Wang, L., Chen, J., Zhang, S., Hong, Y., Yi, H., Wu, D.C., Zhang, Y., Wei, F., Poh,Y.C., Seong, J., Singh, R., Lin, L.J., Doğanay, S., Li, Y., Jia, H., Ha, T., Wang, Y., Huang, B., Wang, N., Matrix softness regulates plasticity of tumour-repopulating cells via H3K9 demethylation and Sox2 expression, Nature Communications 5 (2014) 4619.

[32] N. Strohmeyer, M. Bharadwaj, M. Costell, R. Fässler, D.J. Müller, Fibronectin-bound α5β1 integrins sense load and signal to reinforce adhesion in less than a second, Nature Materials 16 (2017) 1262-1270.

[33] Y. Tan, A.R. Wood, Q. Jia, W. Zhou, J. Luo, F. Yang, J. Chen, J. Chen, J. Sun, J. Seong, A. Tajik, R. Singh, N. Wang, Soft matrices downregulate FAK activity to promote growth of tumor-repopulating cells, Biochemical and Biophysical Research Communications 483 (2017) 456-462.

FIGURE LEGENDS

Figure 1. TRCs do not spread on any TGT surfaces. a, A schematic of a cell on a TGT surface. TGTs with varying T_{tol} ranging from 12 to 56 pN were immobilized on biotinylated BSA passivated glass surfaces via biotin-neutravidin interactions. Biotinylated cyclic-RGDfK peptide, immobilized directly on the surface, was represented as >100 pN. **b**, TRCs adhere to surfaces with $T_{tol} \geq 43$ pN. Interestingly, TRCs do not spread on any TGT surfaces. **c**, Projected cell area of TRCs (n=33, 33, 38, 35 for 43 pN, 50 pN, 56 pN, and >100 pN respectively) are presented in a box-and-whisker plot showing no significant changes across any TGT surfaces (p values are >0.09, 0.07 and 0.99 for 43 pN and 50 pN, 50 pN and 56 pN, and 56 pN and >100 pN, respectively). **d**, A box-and-whisker plot shows a dimensionless parameter-CSI of cells on varying T_{tol} surfaces. No significant changes in CSI values were observed across any TGT surfaces (p values are >0.78, 0.47, 0.29 for 43 pN and 50 pN, 50 pN and 56 pN, and 56 pN and >100 pN, respectively).

Figure 2. Single-mRNA-transcript statistics revealed a dissimilarity in RhoA and Cdc42 expression in TRCs leading to suppression in cell spreading.

a, Representative images showing mRNA-transcript statistics of RhoA, Rac1, and Cdc42 in single control cells and TRCs. **b,** Correlation analysis between RhoA and Cdc42 transcripts (top) and RhoA and Rac1 transcripts (bottom) is shown here. RhoA and Cdc42 expression in control cells are tightly correlated while TRCs tend to exhibit a heterogeneous expression pattern. Each dot represents a single cell (ρ, Pearson correlation coefficient). **c**, RhoA: Cdc42 and RhoA: Rac1 in control cells and TRCs are significantly different ($p< 1.35x10^{-58}$ and $5.86x10^{-13}$ for RhoA: Cdc42 and RhoA: Rac1 respectively).

Figure 3. TRCs' inability to spread corresponds to very few focal adhesions but can be restored by *Cdc42* overexpression. a, Quantification of TIRF microscopy images show very dissimilar FA formation of control cells and TRCs expressing mCherry-vinculin. Color bar represents FA intensity relative to maximum intensity. **b-c**, Histogram plot of FA area in control cells and TRCs is shown here after 1 hour (n= 10 for both control cells and TRCs) and 4 hour (n= 10 and 15 for control cells and TRCs respectively) of cell plating. The number of FAs with area $\geq 1.5\ \mu m^2$ per cell in control cells was significantly different between 1 hour and 4 hour ($p<0.02$), but not in TRCs ($p>0.44$) (insets). **d**, Representative images of TRCs with overexpression of Rac1 and Cdc42 show that Cdc42 alone, but not Rac1, can facilitate cell spreading in TRCs with filopodia-like extensions (inset). A TRC not transfected with Cdc42 did not spread (arrowhead, DIC image; cell boundary, fluorescence image). **e**, Single mRNA-transcripts were quantified after transient overexpression of Cdc42 in TRCs. A representative image of Cdc42-overexpressed-TRC is shown (left). A plot of CSI vs. Cdc42 density is shown in blue representing overexpressed Cdc42 (n=46, Pearson's correlation coefficient $\rho= -0.62$) and red representing endogenous Cdc42 transcripts in TRCs (n=168, $\rho=0.07$). A clear threshold of ~ 25 Cdc42 transcripts per projected cell area is observed for TRC spreading initiation.

Figure 4. Overexpression of Cdc42 in TRCs causes increasing cell spreading capability with increasing T_{tol}. a, TRCs transfected with Cdc42-GFP can spread more with increasing T_{tol}. **b**, Summarized data of Cdc42 overexpressed TRC spreading on 43 pN, 56 pN, and >100 pN surfaces (n= 22, 29, 22 for 43 pN, 56 pN, and >100 pN surfaces respectively). Significant differences in projected cell area were observed between 43pN and 56 pN, and 56 pN and >100

pN ($p< 2.89x10^{-8}$ and $5.43x10^{-6}$ respectively). Similarly, significant differences in CSI between 43pN and 56 pN, and 56 pN and >100 pN were observed ($p< 0.04$ and $9.33x10^{-4}$ respectively).

Fig. 1

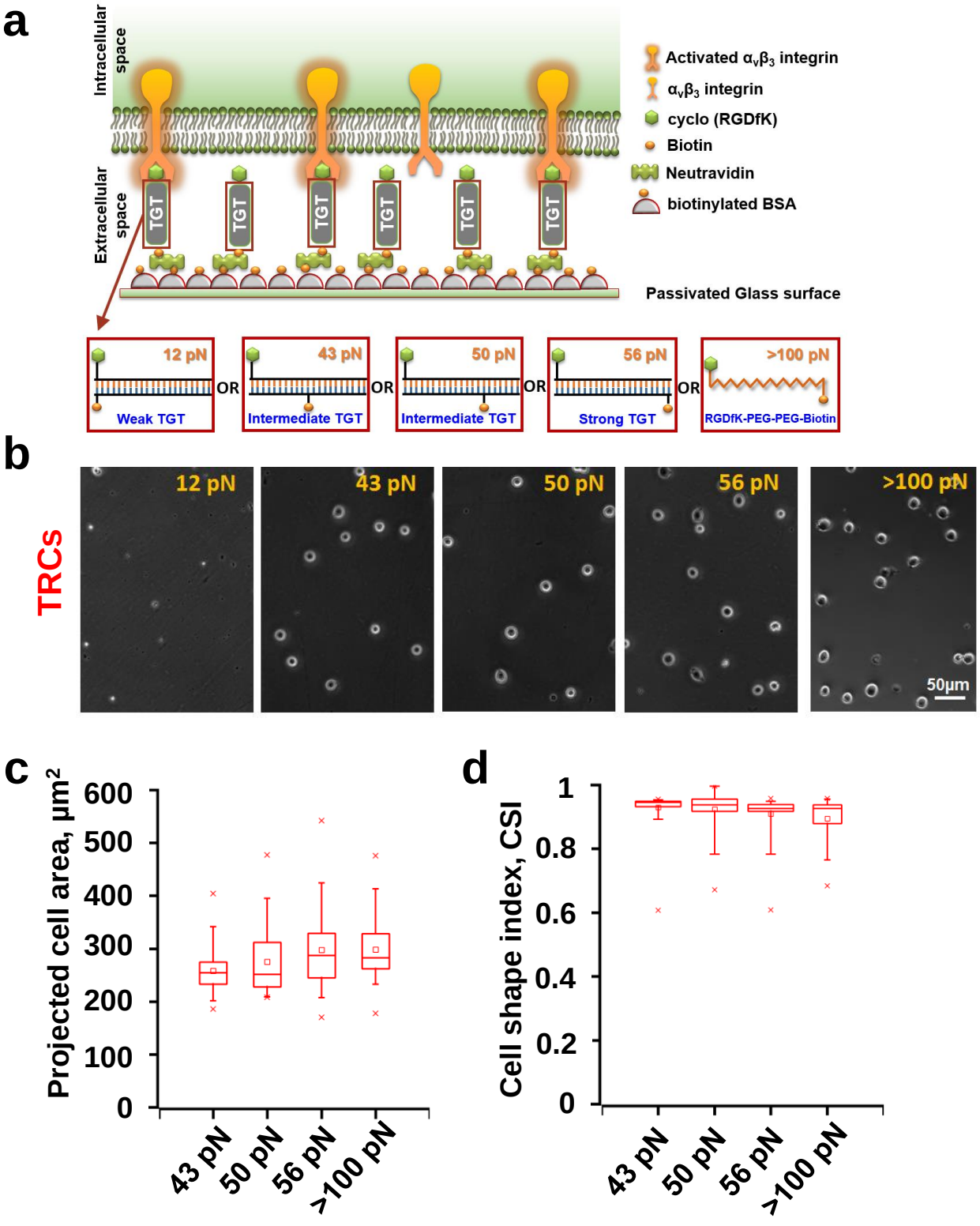
a
Intracellular space
Extracellular space
TGT
Activated $\alpha_v\beta_3$ integrin
$\alpha_v\beta_3$ integrin
cyclo (RGDfK)
Biotin
Neutravidin
biotinylated BSA
Passivated Glass surface
12 pN
Weak TGT
OR
43 pN
Intermediate TGT
OR
50 pN
Intermediate TGT
OR
56 pN
Strong TGT
OR
>100 pN
RGDfK-PEG-PEG-Biotin
b
TRCs
12 pN
43 pN
50 pN
56 pN
>100 pN
50μm
c
Projected cell area, μm²
600
500
400
300
200
100
0
43 pN
50 pN
56 pN
>100 pN
d
Cell shape index, CSI
1
0.8
0.6
0.4
0.2
0
43 pN
50 pN
56 pN
>100 pN

Fig. 2

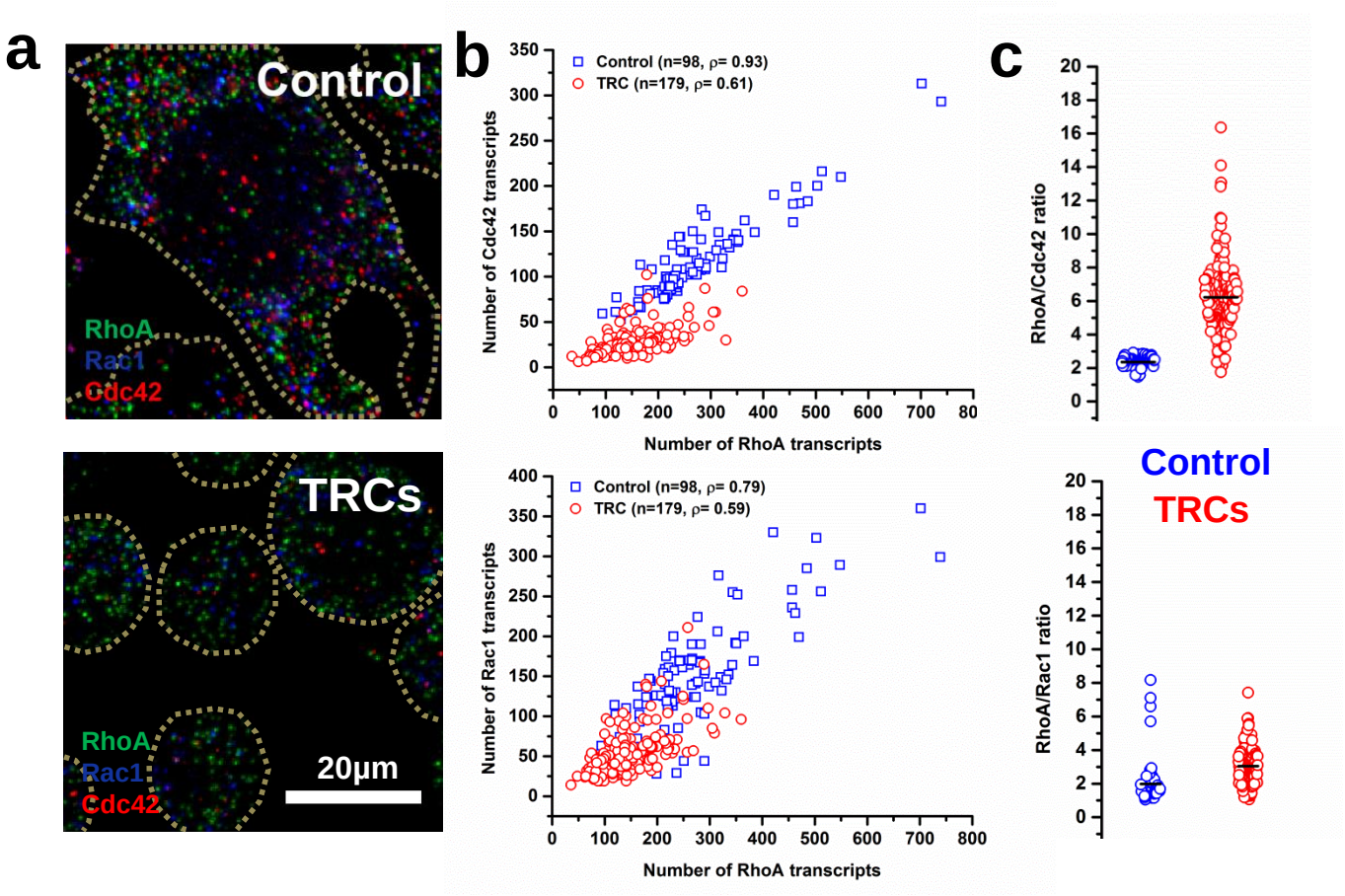
a
Control
RhoA
Rac1
Cdc42
TRCs
RhoA
Rac1
Cdc42
20μm
b
Control (n=98, ρ= 0.93)
TRC (n=179, ρ= 0.61)
Number of Cdc42 transcripts
Number of RhoA transcripts
Control (n=98, ρ= 0.79)
TRC (n=179, ρ= 0.59)
Number of Rac1 transcripts
Number of RhoA transcripts
c
RhoA/Cdc42 ratio
RhoA/Rac1 ratio
Control
TRCs

Fig. 3

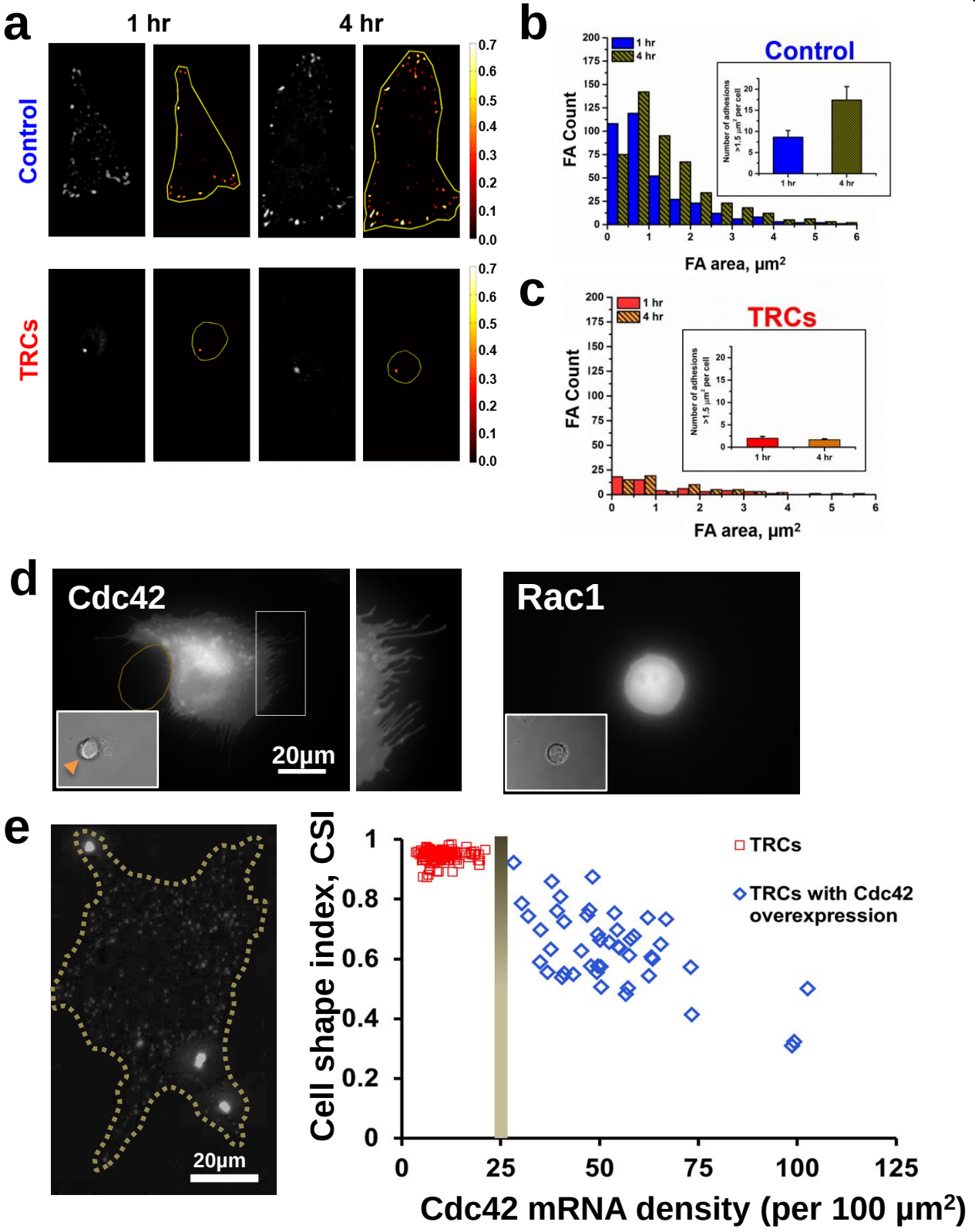
a
1 hr
4 hr
Control
TRCs
0.7
0.6
0.5
0.4
0.3
0.2
0.1
0.0
b
Control
1 hr
4 hr
FA Count
FA area, μm²
Number of adhesions >1.5 μm² per cell
c
TRCs
d
Cdc42
20μm
Rac1
e
20μm
Cell shape index, CSI
Cdc42 mRNA density (per 100 μm²)
TRCs
TRCs with Cdc42 overexpression

a

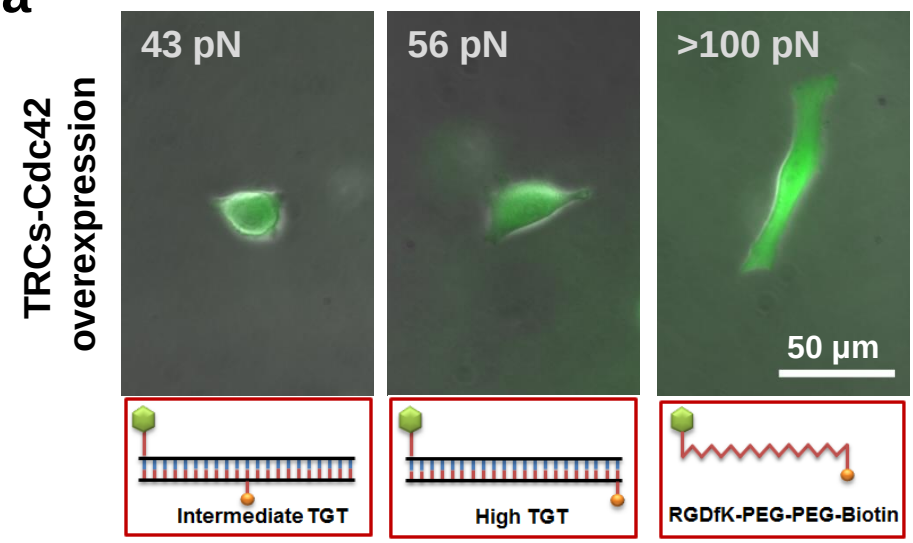
TRCs-Cdc42 overexpression
43 pN
56 pN
>100 pN
50 μm
Intermediate TGT
High TGT
RGDfK-PEG-PEG-Biotin

b

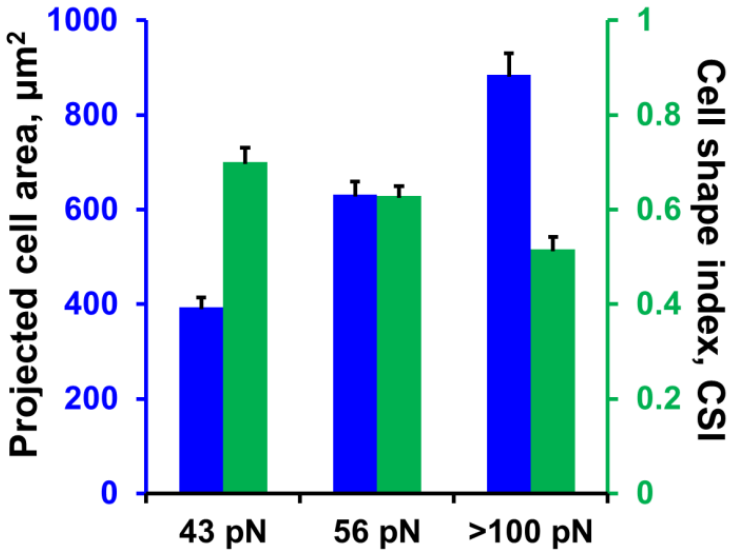
Projected cell area, μm²
1000
800
600
400
200
0
Cell shape index, CSI
1
0.8
0.6
0.4
0.2
0
43 pN
56 pN
>100 pN

SUPPLEMENTAL INFORMATION for

Cdc42-dependent modulation of rigidity sensing and cell spreading in tumor repopulating cells

Farhan Chowdhury[a,*], Sultan Doğanay[b,c,1], Benjamin J. Leslie[d,1,2], Rishi Singh[e], Kshitij Amar[a], Bhavana Talluri[a], Seongjin Park[b], Ning Wang[e], and Taekjip Ha[d,f]

[a] *Department of Mechanical Engineering and Energy Processes, Southern Illinois University Carbondale, Carbondale, IL 62901, U.S.A.*
[b] *Department of Physics, University of Illinois at Urbana-Champaign, Urbana, IL 61801, U.S.A.*
[c] *Center for Biophysics and Computational Biology, University of Illinois at Urbana-Champaign, Urbana, IL 61801, USA*
[d] *Howard Hughes Medical Institute, Johns Hopkins University, Baltimore, MD, 21205, U.S.A.*
[e] *Department of Mechanical Science and Engineering, University of Illinois at Urbana-Champaign, Urbana, IL 61801, U.S.A.*
[f] *Department of Biophysics and Biophysical Chemistry, Johns Hopkins University, Baltimore, MD 21205, U.S.A.*
[1] *Contributed equally.*
[2] *Present address: Department of Biology, The College of Wooster, Wooster, OH, U.S.A*

*Correspondence: farhan.chowdhury@siu.edu (F.C.)

This PDF file includes additional

EXPERIMENTAL PROCEDURES

TRC generation in 3D fibrin gels

Fibrinogen and thrombin (Reagent Proteins), isolated from Salmon, were used for making the 3D-fibrin-gel cell culture. Generation of TRCs with B16-F1 cells, described elsewhere [1], were carried out with minor modification. Briefly, fibrinogen was diluted to 2 mg/ml with T7 buffer (50 mM Tris, 150 mM NaCl, pH adjusted to 7.4). 1:1 ratio of fibrinogen and cell solution mixture finally resulted in 1 mg/ml fibrinogen (90 Pa gel). 3000 cells were seeded in each of the 96 wells and activated with 100 U/ml thrombin. The 96-well plate was then placed into 37°C cell culture incubator for 15 min. Lastly, 200 µl cell culture medium was added into each well. Fresh culture medium was exchanged every two days. TRCs were freshly isolated from 3D fibrin gels on day 5 for experiments.

Treatments, constructs and cell transfection

Cells were transfected in 6-well dishes (9.6 cm^2 well area) with 2.5 µg plasmid DNA and incubated overnight using Lipofectamine LTX with Plus reagent (Invitrogen) following manufacturer's protocol. For monitoring focal adhesions, a plasmid expressing mCherry-vinculin was transfected in control and TRCs. Overexpression of RhoA-EGFP, Rac1-EGFP, and Cdc42-EGFP was carried out with plasmids available from Addgene (plasmid # 23224, 12980, and 12975 respectively). Vector pEGFP-N1 from Clontech was used as a control. For plasmid transfection in TRCs, freshly isolated TRCs from 3D fibrin gels were plated on a 6 well tissue culture dish. After waiting for 4 hours to allow cells to adhere to the surface, cells were transfected with plasmids. After overnight transfection with plasmids, cells were detached from the surface by Trypsin free EDTA solution. Trypsin was specifically not used in the assay as

trypsin digests cell surface proteins including integrins. Isolated cells were plated on glass cover slides engineered with different tension tethers. Cells were incubated on the cover slides for 1 to 4 hours before imaging. Cell imaging of TRCs was carried out within 24 hours of isolation from the 3D fibrin gel unless stated otherwise.

TIRF microscopy and focal adhesion quantification

Control cells and TRCs expressing mCherry-vinculin were seeded on chambered slides passivated by biotin-BSA, incubated with NeutrAvidin, and functionalized by biotinylated cyclic-RGDfK (Peptides International). Images were captured by an inverted epifluorescence microscope (Nikon Eclipse T*i* stabilized by Perfect Focus System) equipped with a 100x NA 1.49 (Nikon APO x100 oil) TIRF objective, a cooled EMCCD camera (Andor DU897), an ASI motorized stage is used for x-y-z position control, and an Agilent laser system (MC400B) with fiber-coupled 561 laser to illuminate the sample. The software for data acquisition was Nikon Elements. For fluorescence imaging, a quad-band dichroic mirror (Chroma, ZT405-488-561-640RPC) and a band-pass emission filter set (600/50) were used for this study. The microscope is also equipped with live cell imaging chamber with temperature controls.

Individual FAs and their characteristics were quantified following methods described earlier [2,3]. Quantification of FA morphology was carried out through a custom MATLAB (Mathworks) program. Fluorescence images were first high-pass filtered, and then used to create binary masks marking FAs. Masks were generated using a threshold equal to 65% of the maximum image brightness. A segmentation algorithm was used to label and measure each FA separately, with regions smaller than 10 pixels assumed to be noise. Segmentation allowed simple quantification of focal adhesion area. Subsequently additional FA properties like aspect ratios were quantified. A best-fit-ellipse was applied to each focal adhesion, allowing

quantification of each FA aspect ratio. Aspect ratio is defined as the length-ratio of the major axis to the minor axis.

Immunofluorescence

For immunofluorescence microscopy, cells were fixed in PBS containing 4% paraformaldehyde, permeabilized with 0.25% Triton X-100, and blocked in PBS containing 2% BSA for 1 hour at room temperature as described earlier [4]. Cells were incubated with primary antibody (Rabbit anti-vinculin, Abcam; Rabbit anti-phospho-Rac1/Cdc42 (Ser71), Bioss Antibodies) at 1:200 dilution followed by incubation with donkey anti-rabbit secondary antibody conjugated with Alexa 647 (Abcam) at a dilution of 1:400.

Quantitative real-time PCR analysis

Total RNA was extracted and purified using Qiagen's RNeasy Mini Kit (Qiagen; cat no. 217004). Purified RNA quantity was measured using a NanoDrop spectrophotometer. mRNA was then converted to cDNA using the BioRad iscript cDNA synthesis kit (Bio-Rad Laboratories, Hercules, CA; cat no. 170-8890). qPCR was performed using Power SYBR Green PCR Master Mix (Applied Biosystems, Warrington, UK; cat no. 4367659). RhoA, Rac1, and Cdc42 mRNA expressions were examined. For relative mRNA analysis, the cycle threshold (C_T) value for samples was determined. These values were normalized with the comparative C_T method with elongation factor alpha1 (Ef1α) for relative gene-expression quantification. The primer sequences are shown in Table S1.

RNA interference

Cells were transfected with Cdc42 siRNA constructs using Lipofectamine 2000 (Invitrogen) as per manufacturer's protocol. Transfected cells were cultured in 24-well plates and assayed 48 hour post transfection. Two Cdc42 siRNA constructs were purchased from Invitrogen (ID # 66023 and 161124). The negative control siRNA was also purchased from Invitrogen (ID #103860). The construct sequences are provided in Table S2.

Single molecule FISH to visualize and quantify mRNA

For *in situ* hybridization, amine functionalized DNA probes for RhoA, Rac1, and Cdc42 mRNA were designed with Stellaris® Probe Designer version 4.0 available from http://www.biosearchtech.com/ (Biosearch Technologies). The amine groups of RhoA, Rac1, and Cdc42 probes were then coupled to the fluorophores Cy3 NHS Ester (GE Healthcare Life Sciences), Alexa 594 NHS Ester (Invitrogen), and Cy5 NHS Ester (GE Healthcare Life Sciences) respectively, according to the dye manufacturers' recommendations. In a separate experiment where overexpressed Cdc42 mRNAs alone were counted, amine reactive Cdc42 probes were conjugated with Cy3 NHS Ester dyes (GE Healthcare Life Sciences). The probes were precipitated twice in EtOH to remove free dye and then HPLC purified on a Phenomenex Oligo Clarity-RP C18 column using a 20-60% linear gradient of 50mM TEAA:MeOH to separate fluorophore-coupled oligos. Cells were seeded on glass surfaces, passivated by biotin-BSA, incubated with NeutrAvidin, and functionalized by RGDfK (Peptides International). The cells were then fixed with 4% formaldehyde for 10 min at room temperature, washed with 1x PBS, and permeabilized overnight with freshly prepared 70% ethanol. The following morning, the cells were rehydrated with a solution of 2x SSC and 10% formamide followed by a 2x SSC wash before *in situ* hybridization. The hybridization reaction was then carried out with hybridization buffer containing 10% dextran sulfate, 0.02% RNase-free BSA, 50 μg E.coli

tRNA, 2 mM vanadyl-ribonucleoside complex, 10% formamide, 2x SSC, and FISH probes specific for RhoA, Rac1 and Cdc42. Following *in situ* hybridization, cells were washed at least twice for 30 min at 37 °C using a wash buffer containing 10% formamide and 2x SSC to remove unbound probes and kept at 4 °C in 2X SSC until imaging. During imaging, a mounting medium containing an oxygen-scavenging system with 10 mM Tris HCl pH 8.0, 1% glucose, glucose oxidase, catalase, and 2x SSC was used. Cells were imaged using a Zeiss Axiovert 200M inverted fluorescence microscope (Zeiss, Germany), equipped with a cooled EMCCD camera (Photometrics, Cascade 512), motorized stage, Xcite illuminator, and a x100 NA 1.46 oil immersion objective. Z-stack images were taken automatically covering entire 3D volume of the cells with 0.3 microns between each slices and an exposure time of 500 milliseconds. To quantify number of mRNAs, we followed the method and software described in a previous study [5].

Data analysis algorithm for single mRNA quantification

When Cdc42 is overexpressed in TRCs, quantification of single mRNA transcripts becomes difficult due to the close proximity of mRNA molecules. Therefore, to quantify overexpressed Cdc42 mRNA transcripts in TRCs, we utilized data analysis algorithm as described here [6].

SUPPLEMENTARY TABLES

Supplementary Table 1. qPCR primer sequences.

	Forward	Reverse
Cdc42	5'-CTC CGC CCT CAC ACA GAA AG-3'	5'-AAG ACA CGA AGA TGC CCC AG-3'
Rac1	5’-GGA GAC GGA GCT GTT GGT AAA-3’	5’-CTT CTT GAC AGG AGG GGG AC-3’
RhoA	5’-AAT GAA GCA GGA GCC GGT AA-3’	5’-GTA CCC AAA AGC GCC AAT CC-3’
Ef1α	5’-ATA TTA CCC CTA ACA CCT GG-3’	5’-CTG TGA CAG ATT TTT GGT CAA-3’

Supplementary Table 2. siRNA sequences.

	Sense	Anti-sense
Control	5'-AGUACUGCUUACGAUACGGTT-3'	5'- CCGUAUCGUAAGCAGUACUTT-3'
Cdc42 siRNA #1	5’-GGGCAAGAGGAUUAUGACATT-3’	5’-UGUCAUAAUCCUCCUCUUGCCCTG-3’
Cdc42 siRNA #2	5’- CCGCUAAGUUAUCCACAGATT-3’	5’-UCUGUGGAUAACUUAGCGGTC-3’

SUPPLEMENTARY FIGURES

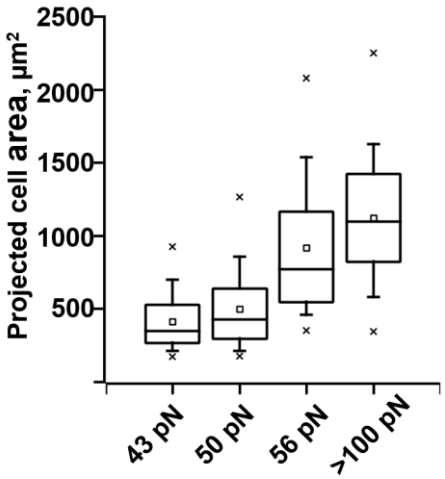

Supplementary Figure 1. Cell spreading area in B16-F1 control cells increases with increasing molecular tension tolerances. Projected area of cell spreading on each TGT surfaces is presented here as a box-whisker plot. Number of data points on each molecular tension tolerance are n=64, 63, 46, 48 for 43 pN, 50 pN, 56 pN, and >100 pN surfaces respectively. Data replotted from Chowdhury et al., 2015 [7].

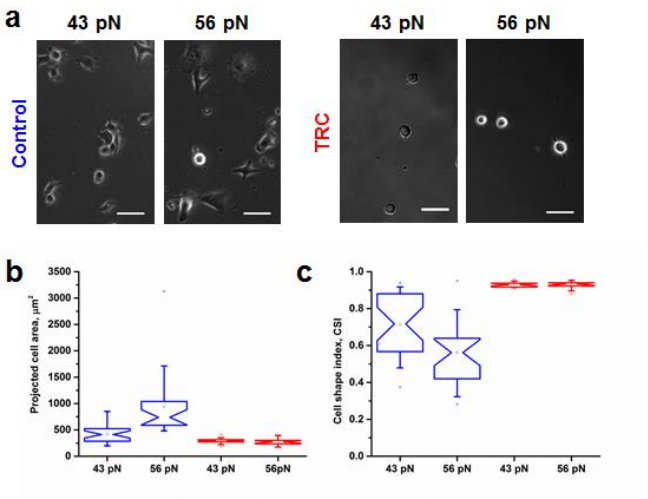

Supplementary Figure 2. Similar to B16-F1 cells, cell spreading area in B16-F10 control cells, but not in TRCs, increases with increasing molecular tension tolerances. (**a**) Representative images of B16-F10 control cells and TRCs on 43 and 56 pN surfaces. (**b**) A box-and-whisker plot shows projected cell spreading area of B16-F10 control cells and TRCs. Cell spreading area of B16-F10 control cells (n=30, 24 for 43 pN and 56 pN surface respectively) increased with increasing tension tolerances while TRCs (n=22, 18 for 43 pN and 56 pN surface respectively) did not spread across tension tolerance surfaces. Significant change in cell area in B16-F10 control cells between 43 pN and 56 pN surface was observed ($p<2.54x10^{-5}$). On the other hand, projected cell spreading area for TRCs did not show any significant differences between 43 pN and 56 pN surfaces ($p >0.24$). (**c**) A box-and-whisker plot shows CSI values for B16-F10 control and TRCs. For B16-F10 control cells, significant changes were observed between 43 pN and 56 pN TGT surface ($p< 0.003$) while CSI values for TRCs did not change significantly between 43 pN and 56 pN ($p> 0.88$). Scale bar, 50 μm.

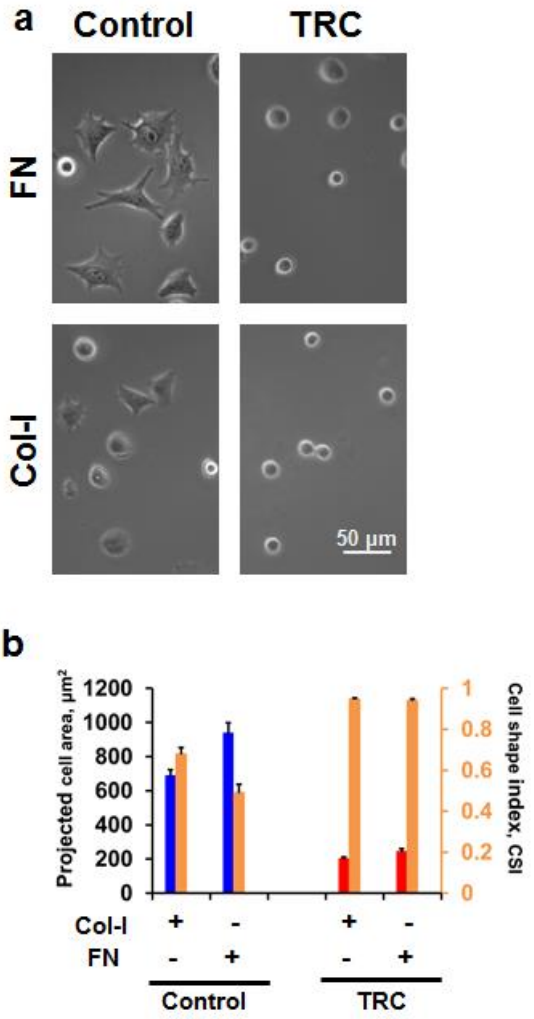

Supplementary Figure 3. Unlike control cells, TRCs do not spread on natural ligands like fibronectin and type-I collagen coated surfaces. (**a**) Cell were plated on rigid dishes coated with fibronectin (10 µg/ml) and type-I collagen (40 µg/ml). TRCs do not spread on any of the natural ligands. (**b**) Control cell spreading area is significantly different than TRCs on both fibronectin (n=26 and 32 for control and TRCs respectively; $p< 3.28x10^{-12}$) and type-I collagen (n=30 and 32 for control and TRCs respectively; $p< 7.73x10^{-16}$). Similar change in CSI values were also observed between control cells and TRC ($p< 1.95x10^{-12}$ and $p<1.48x10^{-10}$ for fibronectin and type-I collagen respectively). Blue bars and red bars represent projected cell area of control cells and TRCs respectively.

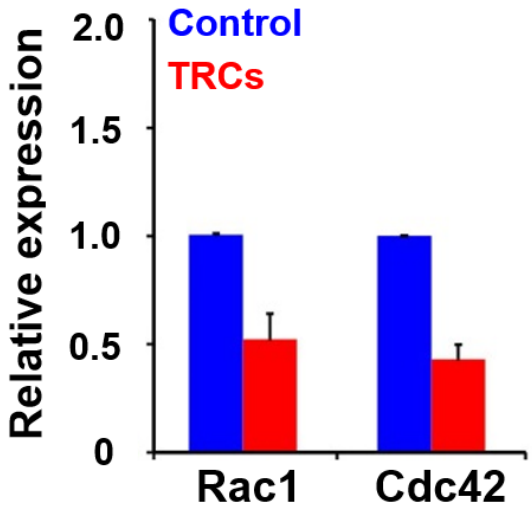

Supplementary Figure 4. Quantitative real-time PCR displays downregulation of *Rac1* and *Cdc42*. Data from three independent experiments. Data represent mean± s.e.m.

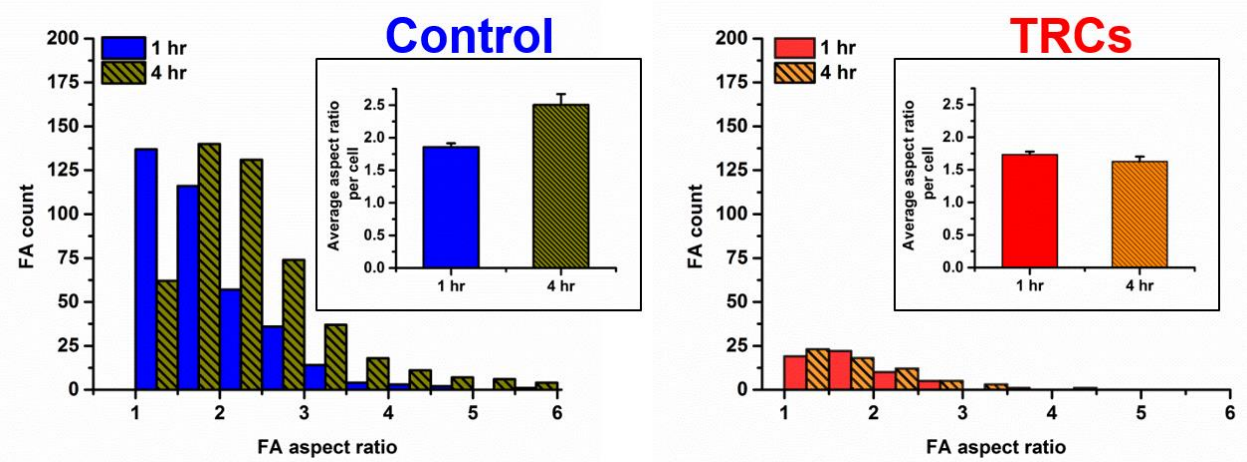

Supplementary Figure 5. Histogram plot of FA aspect ratio in control cells and TRCs after 1 hour (n= 10 for both control cells and TRCs) and 4 hour (n= 10 and 15 for control cells and TRCs respectively) of cell plating. Average FA aspect ratio in control cells was significantly increased at 4 hour ($p<0.001$) (left inset). However, no significant changes in FA aspect ratio were observed in TRCs between 1 hour and 4 hour ($p>0.32$) (right inset).

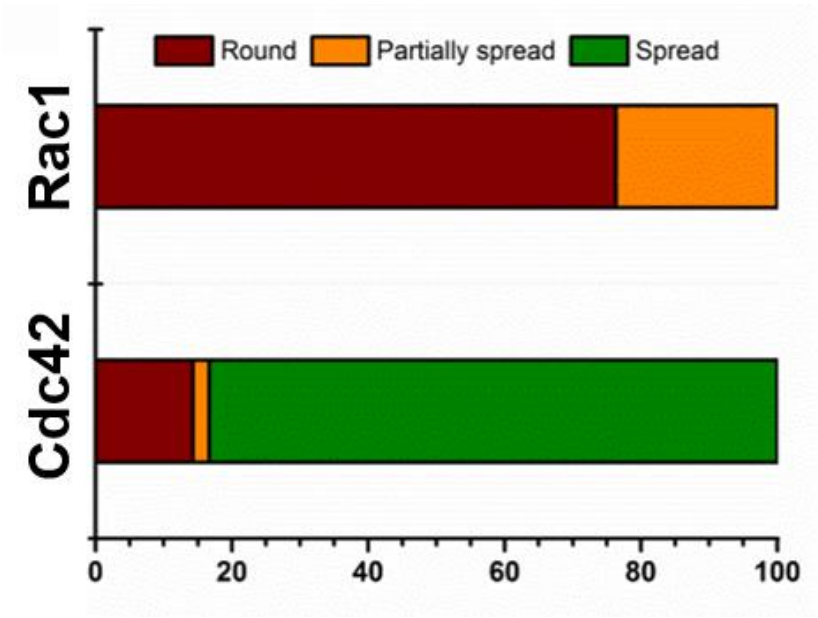

Supplementary Figure 6. Transient overexpression of Cdc42, but not Rac1, induced cell spreading in TRCs. A stacked bar plot indicates a vast majority of TRCs spread with overexpression of Cdc42. However, no cell spreading was observed with Rac1 overexpression.

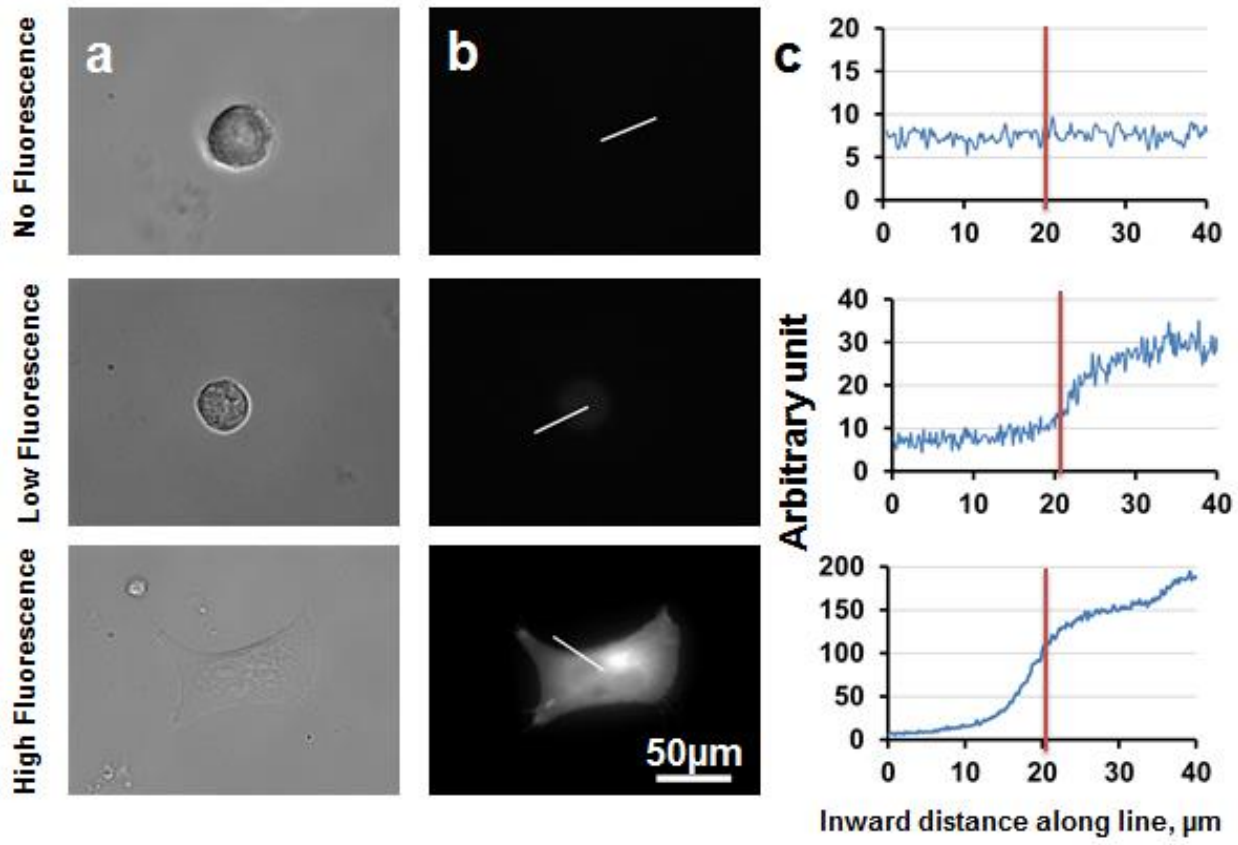

Supplementary Figure 7. Cdc42 dependent cell spreading in TRCs. (**a**-**b**) DIC and fluorescent images of representative TRCs with no fluorescence, low fluorescence, and high fluorescence are shown. White lines were arbitrarily selected for quantifying fluorescent intensities. (**c**) Corresponding line plots are shown. TRCs do not spread when Cdc42 expression is low. It is only when Cdc42 is highly expressed TRCs exhibit cell spreading indicating a possible Cdc42 threshold in TRC spreading. Vertical red lines indicate cell edges.

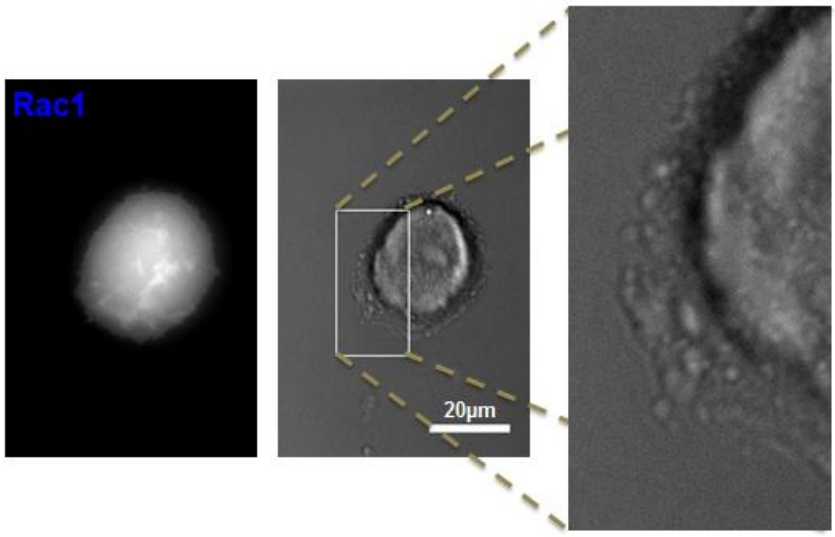

Supplementary Figure 8. Transient overexpression of Rac1 in TRCs induces partial cell spreading in ~20% of cells. A small lamellipodia like extensions, known to be promoted by Rac1, is seen in the inset.

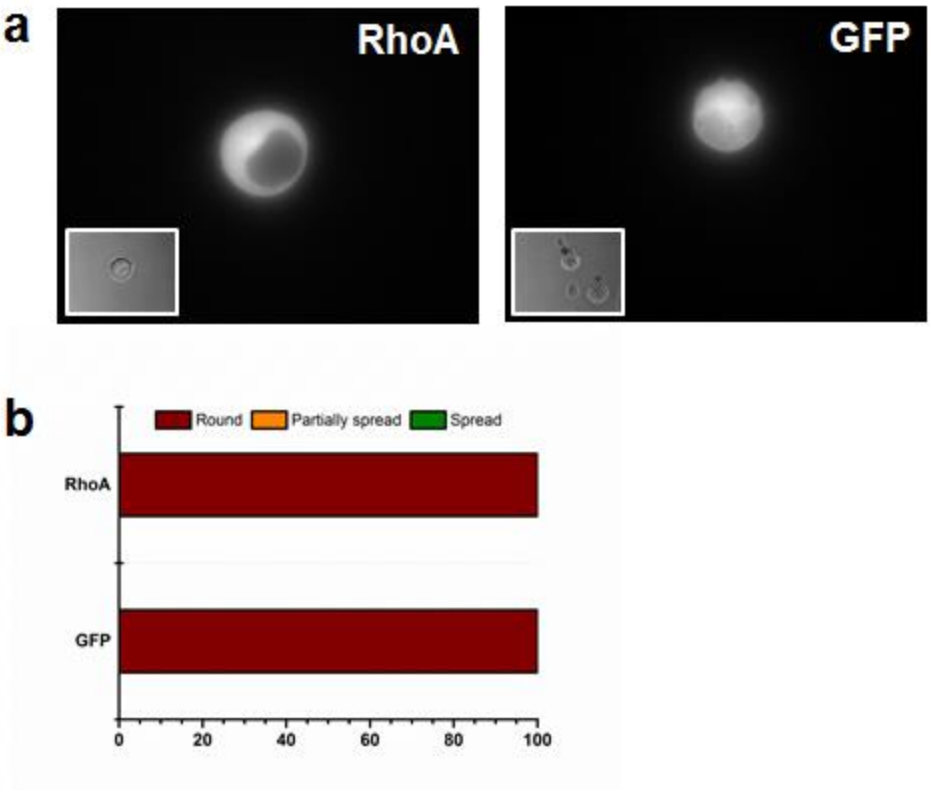

Supplementary Figure 9. Transient overexpression of RhoA and GFP do not induce cell spreading response in TRCs. (**a**) Representative fluorescent and DIC images (inset) of TRCs overexpressing RhoA and GFP is shown. (**b**) No TRCs were found to be spread with overexpression of RhoA and GFP. (n= 34, 8 for RhoA and GFP respectively)

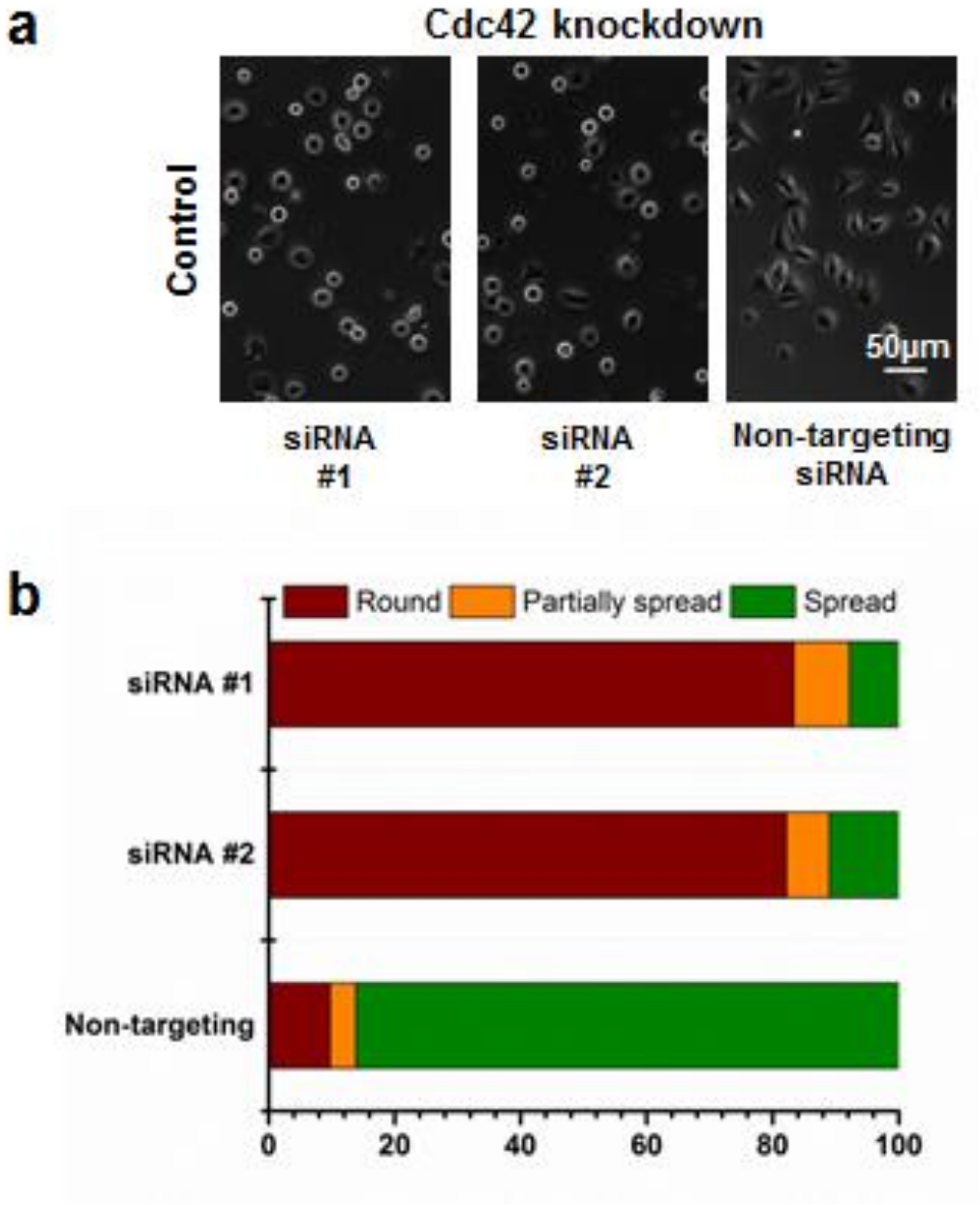

Supplementary Figure 10. siRNA mediated Cdc42 knock down in control cells. (**a**-**b**) Control cells exhibit round morphology, similar to TRCs, with siRNA mediated Cdc42 knock down. Corresponding cell morphology and data summary after Cdc42 knockdown with two different siRNAs are shown. Non-targeting control siRNA did not interfere with cell spreading in control cells.

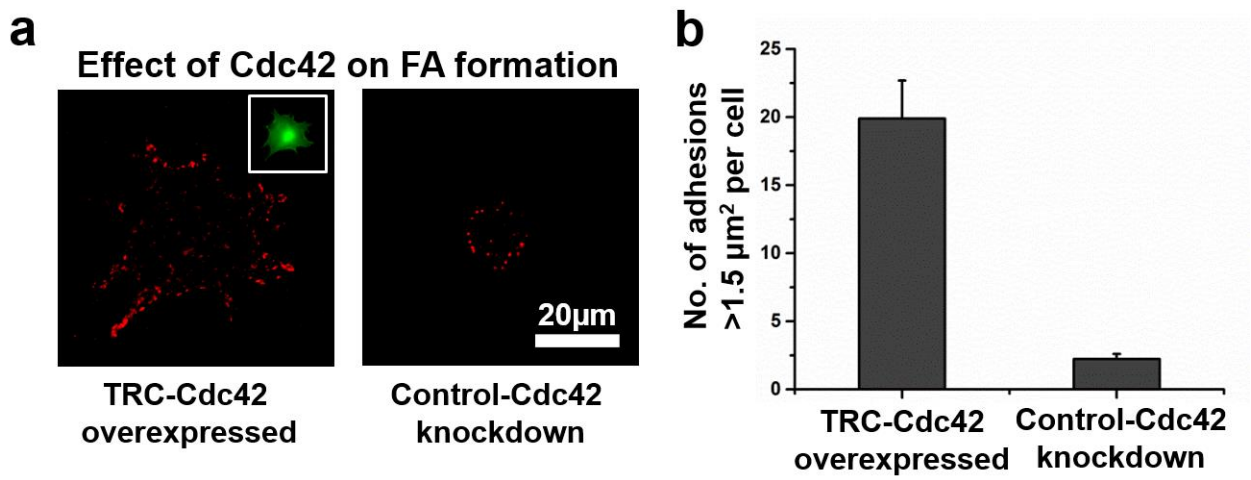

Supplementary Figure 11. Overexpression of Cdc42 in TRCs, in addition to cell spreading, can restore focal adhesion assembly. (**a**) Overexpression of Cdc42 (Cdc42: GFP; inset) can facilitate FA formation in TRCs. Similarly, control cells lose their ability to form FAs when Cdc42 is silenced. Cells were fixed and stained with anti-vinculin primary antibody. Data summary shows number of FAs ≥1.5 μm^2 per cell (n= 10 and 19 for control and TRCs respectively; mean± s.e.m).

REFERENCES

[1] J. Liu, Y. Tan, H. Zhang, Y. Zhang, P. Xu, J. Chen, Y.-C. Poh, K. Tang, N. Wang, B. Huang, Soft fibrin gels promote selection and growth of tumorigenic cells, Nature Materials 11 (2012) 734-741.

[2] P. Kanchanawong, G. Shtengel, A.M. Pasapera, E.B. Ramko, M.W. Davidson, H.F. Hess, C.M. Waterman, Nanoscale architecture of integrin-based cell adhesions, Nature 468 (2010) 580-584.

[3] M.E. Berginski, E.A. Vitriol, K.M. Hahn, S.M. Gomez, High-resolution quantification of focal adhesion spatiotemporal dynamics in living cells, PLoS ONE 6 (2011) e22025.

[4] F. Chowdhury, S. Na, D. Li, Y.C. Poh, T.S. Tanaka, F. Wang, N. Wang, Material properties of the cell dictate stress-induced spreading and differentiation in embryonic stem cells, Nature Materials 9 (2010) 82-88.

[5] A. Raj, P. van den Bogaard, S.A. Rifkin, A. van Oudenaarden, S. Tyagi, Imaging individual mRNA molecules using multiple singly labeled probes, Nat Methods 5 (2008) 877-879.

[6] M.J. Rust, M. Bates, X. Zhuang, Sub-diffraction-limit imaging by stochastic optical reconstruction microscopy (STORM), Nature Methods 3 (2006) 793-795.

[7] F. Chowdhury, I.T. Li, B.J. Leslie, S. Doganay, R. Singh, X. Wang, J. Seong, S.H. Lee, S. Park, N. Wang, T. Ha, Single molecular force across single integrins dictates cell spreading, Integrative Biology 7 (2015) 1265-1271.